Click chemistry expedited radiosynthesis: Sulfur [^{18}F]fluoride exchange of aryl fluorosulfates

Authors:

Qinheng Zheng,[1,5] Hongtao Xu,[2,5] Hua Wang,[1,3,6] Wen-Ge Han Du,[4] Nan Wang,[2] Huan Xiong,[2] Yuang Gu,[2] Louis Noodleman,[4] Guang Yang,[2]* K. Barry Sharpless[1]*, and Peng Wu[3]*

Affiliations:

[1]Department of Chemistry, The Scripps Research Institute, La Jolla, CA 92037, USA.

[2]Shanghai Institute for Advanced Immunochemical Studies (SIAIC), ShanghaiTech University, Shanghai 201210, China.

[3]Department of Molecular Medicine, The Scripps Research Institute, La Jolla, CA 92037, USA.

[4]Department of Integrative Structural and Computational Biology, The Scripps Research Institute, La Jolla, CA 92037, USA.

[5]These authors contributed equally: Qinheng Zheng, Hongtao Xu.

[6]Present address: Sorrento Therapeutics, Inc., San Diego, CA 92121, USA.

*email: sharples@scripps.edu; yangguang@shanghaitech.edu.cn, pengwu@scripps.edu.

Abstract

The lack of simple, efficient [^{18}F]fluorination processes and new target-specific organofluorine probes remains the major challenge of fluorine-18-based positron emission tomography (PET). We report here a fast isotopic exchange method for the radiosynthesis of aryl [^{18}F]fluorosulfate based PET agents enabled by the emerging sulfur fluoride exchange (SuFEx) click chemistry. The method has been applied to the fully-automated ^{18}F-radiolabeling of twenty-five structurally diverse aryl fluorosulfates with excellent radiochemical yield (83–100%) and high molar activity (up to 281 GBq μmol^{-1}) at room temperature in 30 seconds. The purification of radiotracers requires no time-consuming high-performance liquid chromatography (HPLC), but rather a simple cartridge filtration. The utility of aryl [^{18}F]fluorosulfates is demonstrated by the *in vivo* tumor imaging by targeting poly(ADP-ribose) polymerase 1 (PARP1).

Main Text

The non-invasive molecular imaging technique–positron emission tomography (PET), especially that based on the radionuclide fluorine-18, is a widely used technique for tracking biological processes *in vivo*[1-6]. PET imaging has found successful clinical applications in the diagnosis of malignant tumor or neurodegenerative diseases, and the efficacy evaluation of therapeutic treatment. The ever-growing fluorination methodologies over the past decades with a focus on the formation of C–^{18}F bonds sparked the expansion of ^{18}F-based toolbox of radiotracers[7-11].

Despite a few state-of-the-art methods reported to date[12-19], harsh reaction conditions and laborious purification that a common C–^{18}F forming process requires have significantly limited the substrate scope to which fluorine-18 can be introduced. [^{18}F]Fluorodeoxyglucose (FDG), an agent developed half a century ago to map glucose metabolism[20], remains the predominant shareholder of the clinically used PET radiopharmaceuticals.

As noted by Fowler, radiochemists are *working against time*[1] due to the short half-life of fluorine-18 (109.77 min). Taking these challenges into consideration[21], an ideal ^{18}F-radiosynthesis should be: (i) a rapid, mild, and clean ^{18}F-incorporation in the final step of a synthetic sequence; (ii) effective for a diverse spectrum of biologically active organofluorine compounds with reasonable *in vivo* stability; and (iii) compatible with automation. These stringent criteria mirror those set for click chemistry[22].

The newly developed sulfur(VI) fluoride exchange (SuFEx) reactions naturally bridges click chemistry and ^{18}F-radiosynthesis. As demonstrated in the first SuFEx manifesto[23] and subsequent reports, aryl fluorosulfate ($ArOSO_2F$) tops the rank of the stability hierarchy of the most demure electrophiles (*Cf.* sulfonyl fluoride, RSO_2F). This functional group may only become reactive in

the presence of a proper catalyst in organic solvents or upon encountering a specific protein partner, if any, that possess both a nucleophilic amino acid side chain and juxtaposed side chains, e.g. arginine to provide hydrogen bonding networks for the extraction and transport of the departing fluoride in the binding site. In most cases, nevertheless, aryl fluorosulfates simply remain intact in aqueous solutions near neutral conditions in the presence of nucleophilic amino acids, e.g. lysine, serine, threonine, and tyrosine (see Supplementary Information), and even in an entire proteome[24]. Importantly, our proof-of-principle pharmacokinetic evaluations have provided strong evidence of the inertness of several bioactive aryl fluorosulfates *in vivo*[25,26].

On the other hand, one can certainly imagine the possibility of an isotopic exchange event in which the ^{18}F-enriched fluoride anion enables its own nucleophilic displacement of the other fluorine atom of an aryl fluorosulfate[27]. This interchange process may actually be much less energy-demanding than a typical SuFEx reaction with amine or alcohol nucleophiles—the extraneous fluoride anion *per se* compensates the stringent requirements in the latter scenario for the stabilization or solvation of the departing fluoride from an S^{VI}–F site. Significantly, compared to the traditional S_N2-based C–F formation SuFEx with $F^{\ominus}$ might engage the 3d-orbital of S^{VI}, rendering a much lower kinetic barrier[28-33]. Computational study estimated the activation barrier to be 8.8 kcal mol^{-1} (Fig. 1c). Thus, we hypothesize that such a process may take place facilely at room temperature. Given the inertness of many aryl fluorosulfates under physiological conditions, such ^{18}F-labeled aryl fluorosulfates may serve as ideal probes for PET imaging. Here we report the development of a fast ^{18}F-radiolabeling process of preparing aryl fluorosulfate-based probes and their application to PET imaging based on the above principle.

To assess the feasibility of SuFEx between an aryl fluorosulfate and a fluoride salt in solution we performed the ^{19}F nuclear magnetic resonance time-dependent saturation transfer (^{19}F-NMR-

TDST) experiments. The assay developed by Weiss and Spencer[34] enables the differentiation of the "reactant" (left-hand side, Eq. 1, asterisk for clarity) and the "product" (right-hand side) for kinetic rate measurements. In this bimolecular system, the fluoride salt signal ("$F^{\ominus}$*") was irradiated for a set of given saturation times (*TS*). If an intermolecular fluoride exchange process (i.e., SuFEx in Eq. 1) takes place, an apparent drop of the aryl fluorosulfate magnetization (ΔM) would be detected due to saturation transfer (Fig. 2a).

$$PhOSO_2F + "F^{\ominus *}" \overset{SuFEx}{\longleftrightarrow} PhOSO_2F^* + "F^{\ominus}" \quad (1)$$

Toward this end, SuFEx of phenyl fluorosulfate ($PhOSO_2F$, **1**, 0.02 mol L^{-1}) and tetrabutylammonium bifluoride (*n*-$Bu_4N^{\oplus}FHF^{\ominus}$, **2**, 0.2 mol L^{-1}) were evaluated in acetonitrile-*d*3 (MeCN-*d*3). A set of saturation times (TS_i) was applied to the chemical shift of **2** (–150 ppm relative to $CFCl_3$) and the corresponding magnetizations (M_i) of **1** was recorded. Plotting M_i versus TS_i, an exponential decay trend was indeed observed. Using Bloch Equation, the estimated pseudo-first order rate constant was solved with high coefficient of correlation (k_{obs} = 0.16 s^{-1}, R^2 = 0.99) (Fig. 2b). By varying the concentration of **2**, the second-order rate constant of the exchange between **1** and **2** at 298 K was determined, k_{298K} = 0.43 L mol^{-1} s^{-1} (Fig. 2c). Next, an estimation of the exchange barrier was obtained by performing TDST-NMR experiments at various temperatures ranging from 278 to 303 K (Fig. 2d). From Eyring Equation, a low enthalpy of activation (11.3 kcal mol^{-1}) was derived, suggesting the SuFEx process to be a facile reaction at room temperature. Furthermore, Hammett plot analysis was performed, which yielded a positive slope greater than unity (ρ = 1.56), indicating the emergence of negative charge during the reaction pathway (Fig. 2e).

In parallel, we studied several factors that could influence the SuFEx process. Borosilicate glass, of which normal NMR tubes are made, showed no significant inhibition or acceleration

when compared to a plastic reaction vessel (see Supplementary Information). By contrast, solvent had significant impact on the rate of fluoride exchange. The use of a polar, aprotic solvent, such as *N*-Methyl-2-pyrrolidone (NMP), *N*,*N*-dimethylformamide (DMF), dimethyl sulfoxide (DMSO), or MeCN was found to be essential for achieving a fast SuFEx process (see Supplementary Information).

With tetrabutylammonium as the cation, we screened different fluoride anions (Fig. 2f). We found that "basic" fluoride is more effective than its derivatives complexed by Brønsted or Lewis acids (**2**–**5**). Tetrabutylammonium fluoride (**6**•$3H_2O$), although in its trihydrate form, exhibited the highest exchange rate, which is approximately 50-fold faster than that of **2**. Results from density functional theory (DFT) calculation (*vide supra*) suggested that the "naked" fluoride anion (**6**) is much more active than its bifluoride counterpart (**2**), $\Delta G_{calc}^{\ddagger}$(**6**) = 10.5 kcal mol^{-1} (*Cf.* $\Delta G_{exp}^{\ddagger}$ (**2**) = 17.7 kcal mol^{-1}).

Subsequently, counter ions of bifluoride salts were investigated. Finely powdered potassium bifluoride alone did not effect the fluoride exchange in MeCN, albeit its complexes with 18-crown-6 (**7**) or 2.2.2-cryptand (**8**) showed moderate exchange rates. In line with our earlier observation that tris(dimethylamino)sulonium ($TAS^{\oplus}$) was a superior cation for SuFEx reactions[35], the same salt (**10**) showed 10-fold increase in exchange rate compared with **2**.

With kinetic parameters of SuFEx between phenyl fluorosulfate and fluoride salts determined, we embarked on the development of a procedure for incorporating the radioactive [^{18}F]fluoride into aryl fluorosulfates using a fully-automated radiosynthesizer. 3-Ethynylphenyl fluorosulfate (**11**) was chosen as the first target for this endeavor. In a typical experiment, 3-ethynylphenyl fluorosulfate (**11**, 0.1 mg, 0.5 μmol) in MeCN (0.5 mL) was added to azeotropically dried potassium [^{18}F]fluoride (~3.7 GBq) in the presence of 2.2.2-cryptand (**8**). The "full conversion" of

[^{18}F]F$^{\ominus}$ was achieved in 30 seconds at room temperature, showing a single ^{18}F-labeled **11** peak on the crude HPLC traces (Fig. 3a, b). The radiochemical yield (RCY) based on crude HPLC[36] was 99.3 ± 0.6% (four replicates). Followed by a less-than-one-minute C18-cartridge filtration aryl [^{18}F]fluorosulfate product [^{18}F]**11** was isolated. As a comparison, a normal C–^{18}F bond formation reaction usually takes place at >100 ºC, and requires 10–30 min for the reaction and 5–15-min for the HPLC purification[37,38]. To our knowledge, the SuFEx-enabled ^{18}F-radiolabeling, i.e. [^{18}F]SuFEx, is the fastest ^{18}F-incorporation process to date.

Using this strategy, we successfully synthesized twenty five new aryl [^{18}F]fluorosulfates (Fig. 3c), including [^{18}F]fluorosulfate derivatives of nucleosides, e.g. thymidine (**21**), aromatic amino acids, e.g. tyrosine (**23**), and [^{18}F]aryl fluorosulfates (**14**–**20**) bearing orthogonally reactive groups as modular positron-emitting tags for functionalizing biomacromolecules. All [^{18}F]SuFEx reactions afforded excellent radiochemical yields (RCY). Likewise, the ^{18}F-isotopologue of a human soluble epoxide hydrolase (hsEH) inhibitor (*S*)-**24**[25], and a selective estrogen receptor degrader **28** were also synthesized *via* this approach. Aryl fluorosulfates **29**–**34** with potential central nervous system (CNS) targets were synthesized and radiolabeled using the late-stage [^{18}F]SuFEx protocol with excellent RCY.

The ^{18}F-labeled aryl fluorosulfate (*S*)-**24**, was used to assess the *in vivo* stability of the ArOSO$_2$–F group. Upon injection into wt C57BL/6 mice *via* the intravenous (i.v.) route, this compound was found to be mainly enriched in liver where sEH is most abundantly expressed (see Supplementary Information). Importantly, we did not detect apparent ^{18}F-associated signal in the bone—^{18}F bone deposition would indicate the release of [^{18}F]F$^{\ominus}$[39] from the aryl [^{18}F]fluorosulfate *via* a substitution or hydrolytic reaction. The absence of any ^{18}F-associated signal in the bone provides a strong evidence of the *in vivo* stability of this aryl [^{18}F]fluorosulfate.

To apply aryl [^{18}F]fluorosulfates to *in vivo* PET imaging, we synthesized compound **35** by adding a pendent aryl fluorosulfate to the solvent-exposed site of olaparib[40], an FDA-approved anti-cancer drug that inhibits poly(ADP-ribose) polymerase 1 (PARP1). The IC_{50} of **35** against PARP1 was determined to be 32.2 nM (Fig. 4a). Mass spectrometry analysis did not detect covalent adduct formation when recombinant PARP1 was incubated with **35**, which suggests that compound **35** functions as a non-covalent PARP1 inhibitor. In addition, **35** survived "refluxing aniline" test and aqueous buffer stability test, suggesting that this compound has considerable stability in aqueous mixtures. Importantly, **35** also exhibited similar stability as olaparib in the serum of healthy human donors (Fig. 4b). In a Curie-scale radiosynthesis, [^{18}F]**35** was prepared with molar activity (A_m) up to 281 GBq μmol^{-1} (7.59 Ci μmol^{-1}, decay corrected).

A human breast cancer xenograft model was used to assess the ^{18}F-labeled **35** for *in vivo* PET imaging. [^{18}F]**35** was i.v. injected into nude mice of subcutaneous human breast cancer xenograft established using MCF-7, a human breast cancer cell line with upregulated PARP1 expression. The intensive accumulation of the ^{18}F-labeled olaparib analog in tumors were clearly visualized with excellent target-to-background ratio after injection (Fig. 4c, e). In a competition experiment, olaparib (IC_{50} = 2.88 nM) was dosed before i.v. injection of the [^{18}F]**35**, which blocked the accumulation of **35** in tumor, resulting in significant decrease in the ratio of % ID/g (injected dose per gram) of tumor-to-muscle from 2.02 ± 0.70 to 0.79 ± 0.04 ($P < 0.05$) (Fig. 4f), strongly supporting the specificity of this probe. During these experiments, we also detected significant ^{18}F-associated signals in the bone marrow that has abundant PARP1 expression[41,42].

In summary, we have demonstrated a rapid exchange reaction between [^{18}F]F$^{\ominus}$ and the otherwise inert aryl fluorosulfate. *Via* this process, an extremely fast, clean and reliable method for the radiosynthesis of a new class of PET agents—aryl [^{18}F]fluorosulfates is developed and

applied to *in vivo* PET imaging in a xenograpft tumor model. We envisage that useful aryl [^{18}F]fluorosulfates, including those targeting the more challenging CNS, will emerge in the near future.

Acknowledgements

This work is supported by the U.S. National Institutes of Health (R01GM117145 to K.B.S., R01GM093282 to P.W., R01GM100934 to L.N.), the U.S. National Science Foundation (CHE-1610987 to K.B.S.) and ShanghaiTech University startup fund (G.Y.). Q.Z. is an Ellen Browning Scripps Graduate Fellow. We thank Huayi Isotopes Co. (Changshu, Jiangsu Province, China) for access of cyclotron and PET-CT, Dr. Dee-Hua Huang (Scripps NMR Facility) for assistance on TDST-NMR experiments, Prof. Jin-Quan Yu (Scripps) for access of glovebox and GC-EI-MS, Dr. Yongxuan Su (UCSD) for assistance on APCI-MS. We are grateful to Prof. Jiajia Dong (SIOC) for helpful discussion.

Author contributions: K.B.S., P.W., H.W. and Q.Z. conceived the work. Q.Z., and H.W. designed and executed TDST-NMR study. Q.Z. carried out chemical syntheses and characterizations. Q.Z., H.Xu and P.W. designed bioassays. Q.Z. and H.Xu designed and executed radiosynthesis and PET imaging. N.W., and H.Xiong synthesized and assayed PARP1 inhibitors. W.-G.H.D., and L.N. performed computational study. Q.Z., P.W., and K.B.S. wrote the manuscript; H.Xu, and G.Y. assisted with editing.

Data and materials availability: Experimental procedures for chemical and radiosynthesis, ^{1}H-NMR, ^{13}C-NMR, ^{19}F-NMR, ^{19}F-TDST-NMR spectra, analytical HPLC radioactivity and UV

chromatograms, PET-CT images, immunohistochemistry, and DFT calculations are available in the Supplementary Information.

Reference

1 Fowler, J. S. & Wolf, A. P. Working against time: Rapid radiotracer synthesis and imaging the human brain. *Accounts Chem Res* **30**, 181-188 (1997).

2 Phelps, M. E. Positron emission tomography provides molecular imaging of biological processes. *P Natl Acad Sci USA* **97**, 9226-9233 (2000).

3 Gambhir, S. S. Molecular imaging of cancer with positron emission tomography. *Nat Rev Cancer* **2**, 683-693 (2002).

4 Tsien, R. Y. Imagining imaging's future. *Nat Rev Mol Cell Bio*, SS16-SS21 (2003).

5 Willmann, J. K., van Bruggen, N., Dinkelborg, L. M. & Gambhir, S. S. Molecular imaging in drug development. *Nat Rev Drug Discov* **7**, 591-607 (2008).

6 Ametamey, S. M., Honer, M. & Schubiger, P. A. Molecular imaging with PET. *Chem Rev* **108**, 1501-1516 (2008).

7 Cai, L. S., Lu, S. Y. & Pike, V. W. Chemistry with [F-18]fluoride ion. *Eur J Org Chem*, 2853-2873 (2008).

8 Tredwell, M. & Gouverneur, V. 18F Labeling of Arenes. *Angew Chem Int Edit* **51**, 11426-11437 (2012).

9 Brooks, A. F., Topczewski, J. J., Ichiishi, N., Sanford, M. S. & Scott, P. J. H. Late-stage [F-18]fluorination: new solutions to old problems. *Chem Sci* **5**, 4545-4553 (2014).

10 Liang, S. H. & Vasdev, N. C(sp(3))-F-18 Bond Formation by Transition-Metal-Based [F-18]Fluorination. *Angew Chem Int Edit* **53**, 11416-11418 (2014).

11 Preshlock, S., Tredwell, M. & Gouverneur, V. F-18-Labeling of Arenes and Heteroarenes for Applications in Positron Emission Tomography. *Chem Rev* **116**, 719-766 (2016).

12 Lee, E. *et al.* A Fluoride-Derived Electrophilic Late-Stage Fluorination Reagent for PET Imaging. *Science* **334**, 639-642 (2011).

13 Huiban, M. *et al.* A broadly applicable [F-18]trifluoromethylation of aryl and heteroaryl iodides for PET imaging. *Nat Chem* **5**, 941-944 (2013).

14 Graham, T. J. A., Lambert, R. F., Ploessl, K., Kung, H. F. & Doyle, A. G. Enantioselective Radiosynthesis of Positron Emission Tomography (PET) Tracers Containing [F-18]Fluorohydrins. *J Am Chem Soc* **136**, 5291-5294 (2014).

15 Rotstein, B. H., Stephenson, N. A., Vasdev, N. & Liang, S. H. Spirocyclic hypervalent iodine(III)-mediated radiofluorination of non-activated and hindered aromatics. *Nat Commun* **5**, doi:ARTN 436510.1038/ncomms5365 (2014).

16 Sergeev, M. E., Morgia, F., Lazari, M., Wang, C. & van Dam, R. M. Titania-Catalyzed Radiofluorination of Tosylated Precursors in Highly Aqueous Medium. *J Am Chem Soc* **137**, 5686-5694 (2015).

17 Neumann, C. N., Hooker, J. M. & Ritter, T. Concerted nucleophilic aromatic substitution with F-19(-) and F-18(-). *Nature* **534**, 369-373 (2016).

18 Levin, M. D. *et al.* A catalytic fluoride-rebound mechanism for C(sp(3))-CF3 bond formation. *Science* **356**, 1272-1275 (2017).

19 Chen, W. *et al.* Direct arene C-H fluorination with (18)F(-) via organic photoredox catalysis. *Science* **364**, 1170-1174 (2019).

20 Ido, T. *et al.* Labeled 2-Deoxy-D-Glucose Analogs - F-18-Labeled 2-Deoxy-2-Fluoro-D-Glucose, 2-Deoxy-2-Fluoro-D-Mannose and C-14-2-Deoxy-2-Fluoro-D-Glucose. *J Labelled Compd Rad* **14**, 175-183 (1978).

21 Campbell, M. G. *et al.* Bridging the gaps in F-18 PET tracer development. *Nat Chem* **9**, 1-3 (2017).

22 Kolb, H. C., Finn, M. G. & Sharpless, K. B. Click chemistry: Diverse chemical function from a few good reactions. *Angew Chem Int Edit* **40**, 2004-2021 (2001).

23 Dong, J. J., Krasnova, L., Finn, M. G. & Sharpless, K. B. Sulfur(VI) Fluoride Exchange (SuFEx): Another Good Reaction for Click Chemistry. *Angew Chem Int Edit* **53**, 9430-9448 (2014).

24 Chen, W. *et al.* Arylfluorosulfates Inactivate Intracellular Lipid Binding Protein(s) through Chemoselective SuFEx Reaction with a Binding Site Tyr Residue. *J Am Chem Soc* **138**, 7353-7364 (2016).

25 Dong, J., Krasnova, L. & Sharpless, K. B. Fluorosulfonyl sEH Inhibitors. WO2015/188060 (2015).

26 Liu, Z. L. *et al.* SuFEx Click Chemistry Enabled Late-Stage Drug Functionalization. *J Am Chem Soc* **140**, 2919-2925 (2018).

27 Alauddin, M. M. *et al.* Stereospecific fluorination of 1,3,5-tri-O-benzoyl-alpha-D-ribofuranose-2-sulfonate esters: preparation of a versatile intermediate for synthesis of 2 '-[F-18]-fluoro-arabinonucleosides. *J Fluorine Chem* **106**, 87-91 (2000).

28 Bernard-Gauthier, V. *et al.* From Unorthodox to Established: The Current Status of F-18-Trifluoroborate- and F-18-SiFA-Based Radiopharmaceuticals in PET Nuclear Imaging. *Bioconjugate Chem* **27**, 267-279 (2016).

29 Pascali, G. *et al.* Sulfur - fluorine bond in PET radiochemistry. *EJNMMI Radiopharm Chem* **2**, 9 (2017).

30 Ting, R., Adam, M. J., Ruth, T. J. & Perrin, D. M. Arylfluoroborates and alkylfluorosilicates as potential PET imaging agents: High-yielding aqueous biomolecular F-18-labeling. *J Am Chem Soc* **127**, 13094-13095 (2005).

31 Schirrmacher, R. *et al.* F-18-labeling of peptides by means of an organosilicon-based fluoride acceptor. *Angew Chem Int Edit* **45**, 6047-6050 (2006).

32 Bernard-Gauthier, V. *et al.* (1)(8)F-labeled silicon-based fluoride acceptors: potential opportunities for novel positron emitting radiopharmaceuticals. *Biomed Res Int* **2014**, 454503 (2014).

33 Liu, Z. B. *et al.* An Organotrifluoroborate for Broadly Applicable One-Step F-18-Labeling. *Angew Chem Int Edit* **53**, 11876-11880 (2014).

34 Taitelbaum, H., Weiss, G. H. & Spencer, R. G. S. Optimization of Magnetization-Transfer Experiments for Kinetic Rate Measurements. *Nmr Biomed* **7**, 287-292 (1994).

35 Gao, B. *et al.* Bifluoride-catalysed sulfur(VI) fluoride exchange reaction for the synthesis of polysulfates and polysulfonates. *Nat Chem* **9**, 1083-1088 (2017).

36 Coenen, H. H. *et al.* Consensus nomenclature rules for radiopharmaceutical chemistry - Setting the record straight. *Nucl Med Biol* **55**, V-Xi (2017).

37 Scott, P. J. H. & Hockley, B. G. *Radiopharmaceuticals for positron emission tomography*. (Wiley, 2012).

38 Scott, P. J. H. *Radiochemical syntheses; volume 2* (Wiley, Hoboken, New Jersey, 2015).

39 Grant, F. D. *et al.* Skeletal PET with 18F-fluoride: applying new technology to an old tracer. *J Nucl Med* **49**, 68-78 (2008).

40 Dawicki-McKenna, J. M. *et al.* PARP-1 Activation Requires Local Unfolding of an Autoinhibitory Domain. *Mol Cell* **60**, 755-768 (2015).

41 Uhlen, M. *et al.* Proteomics. Tissue-based map of the human proteome. *Science* **347**, 1260419 (2015).

42 Human Protein Atlas. *PARP1*, URL: https://www.proteinatlas.org/ENSG00000143799-PARP1/tissue.

Figure Legends

Fig. 1 | [^{18}F]SuFEx. a, Mechanistic rationale of three strategies for nucleophilic ^{18}F-incorporation and the estimated activation energy (E_a). **b**, Proposed SuFEx of fluorine atom between anionic fluoride and phenyl fluorosulfate (**1**). **c**, Energy profile obtained by density functional theory (DFT) calculations suggests a low barrier for fluoride exchange. **d**, Optimized geometry of the pentacoordinated SuFEx intermediate (INT). Color scheme: C, gray; H, white; O, red; S, yellow; F, green.

Fig. 2 | Intermolecular SuFEx between a nucleophilic fluoride donor and an aryl fluorosulfate. a, Schematic illustration of using time-dependent saturation transfer (TDST)-NMR to monitor intermolecular SuFEx between a nucleophilic fluoride donor and an aryl fluoropsulfate. "F⊖" refers to any nucleophilic fluoride donors, exemplified by those shown below (**f**). **b**, A representative plot of magnetization versus saturation time, and overlapped spectra of the corresponding experiments with saturation time ranging from 0.01 s to 25 s. Conditions: phenyl fluorosulfate (**1**, 0.02 mol L^{-1}), tetrabutylammonium bifluoride (**2**, 0.2 mol L^{-1}), MeCN-*d*3, 298 K. **c**, Measurement of the second-order rate of the SuFEx reaction between **1** and **2**, k_{298K} = 0.43 L mol^{-1} s^{-1} (R^2 = 0.99). **d**, Erying plot of the SuFEx reaction between **1** and **2**. The calculated activation enthalpy was determined, $\Delta H^{\ddagger}_{calc}$ = 11.3 kcal mol^{-1} (R^2 = 0.99). **e**, Hammett plot of the SuFEx reactions between **2** and para-X-substituted phenyl fluorosulfates, ρ = 1.56 (R^2 = 0.93). **f**, Pseudo-first-order rate constants for the SuFEx reaction of **1** using various fluoride salts as nucleophilic fluoride donors. *No exchange detected on NMR.

Fig. 3 | [^{18}F]SuFEx of aryl fluorosulfates: reaction condition and substrate scope. a, [^{18}F]SuFEx reaction of 3-ethynylphenyl fluorosulfate (**11**). Conditions: Compound **11** (0.1 mg, 200 nmol), K[^{18}F]F (ca. 3.7 GBq), 2.2.2-cryptand, K_2CO_3, MeCN (0.5 mL), 23 ºC, 30 s. RCYs

were determined by HPLC after the reaction crude being quenched by water (0.1 mL). **b**, Representative HPLC chromatograms of a reaction crude of [^{18}F]**11**, with UV absorption (gray) and radioactivity (black) traces. **c**, Substrate scope of the [^{18}F]SuFEx reaction following the conditions described before (**a**). *Conditions for Curie-scale synthesis of [^{18}F]**35**: Compound **35** (0.1 mg, 17.2 nmol), K[^{18}F]F (~110 GBq), 2.2.2-cryptand, K_2CO_3, MeCN (10 mL), 23 ºC, 30 s.

Fig. 4 | PET imaging using [^{18}F]35. **a**, Compound **35** is a PARP1 inhibitor, IC_{50} = 32.2 nM. **b**, The serum stability of Compound **35** is comparable to that of olaparib. **c**, Whole body coronal (left), and transvers (right) PET/CT images of human MCF-7 bearing nude mice (transplanted under right shoulder, see white dashed circles) acquired by performing a 55 min dynamic scan following [^{18}F]**35** administration. **d**, Transvers PET/CT image of mice pre-treated with excess olaparib 30 min before [^{18}F]**35** administration. No significant uptake of [^{18}F]**35** was observed at the tumor site. **e**, Time plot of percentage of injected dose per gram (%ID/g) of tissue of interest. Error bars represent the mean plus standard deviation (SD, N = 3). P-values were calculated by unpaired Student's t-test; *$P < 0.05$. **f**, Comparison of pre-treatment with either vehicle (N = 3) or 50 mg/kg or olaparib (N = 3) on the %ID/g ratio of tumor versus muscle (healthy tissue).

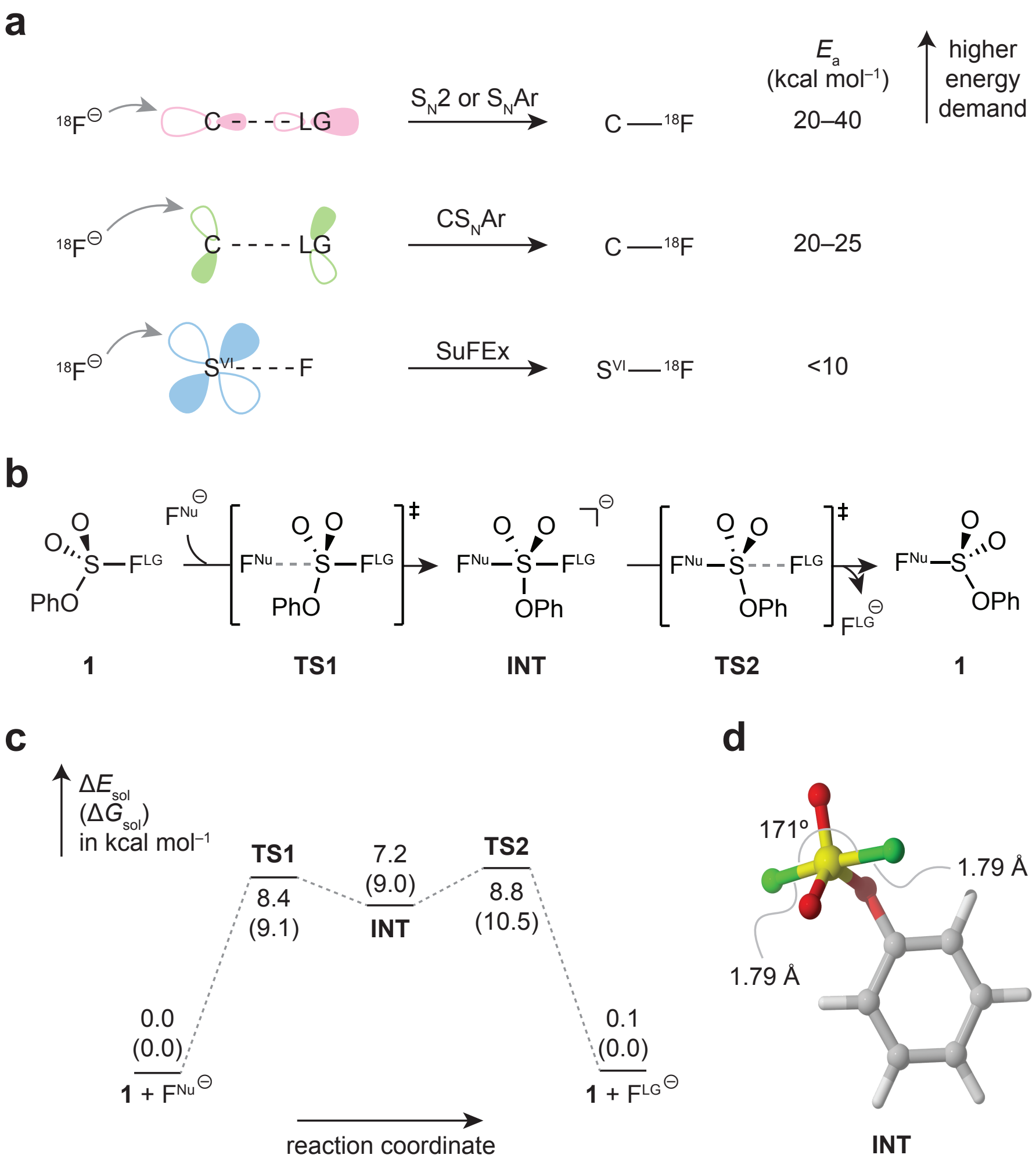
a
E_a (kcal mol^{-1})
higher energy demand
$^{18}F^{\ominus}$
C - - - - LG
S_N2 or S_NAr
C — ^{18}F
20–40
CS_NAr
20–25
S^{VI} - - - - F
SuFEx
S^{VI} — ^{18}F
<10
b
F^{Nu}
PhO
F^{LG}
OPh
1
TS1
INT
TS2
1
c
ΔE_{sol} (ΔG_{sol}) in kcal mol^{-1}
TS1
8.4 (9.1)
7.2 (9.0)
INT
TS2
8.8 (10.5)
0.0 (0.0)
1 + F^{Nu}
0.1 (0.0)
1 + F^{LG}
reaction coordinate
d
171°
1.79 Å
1.79 Å
INT

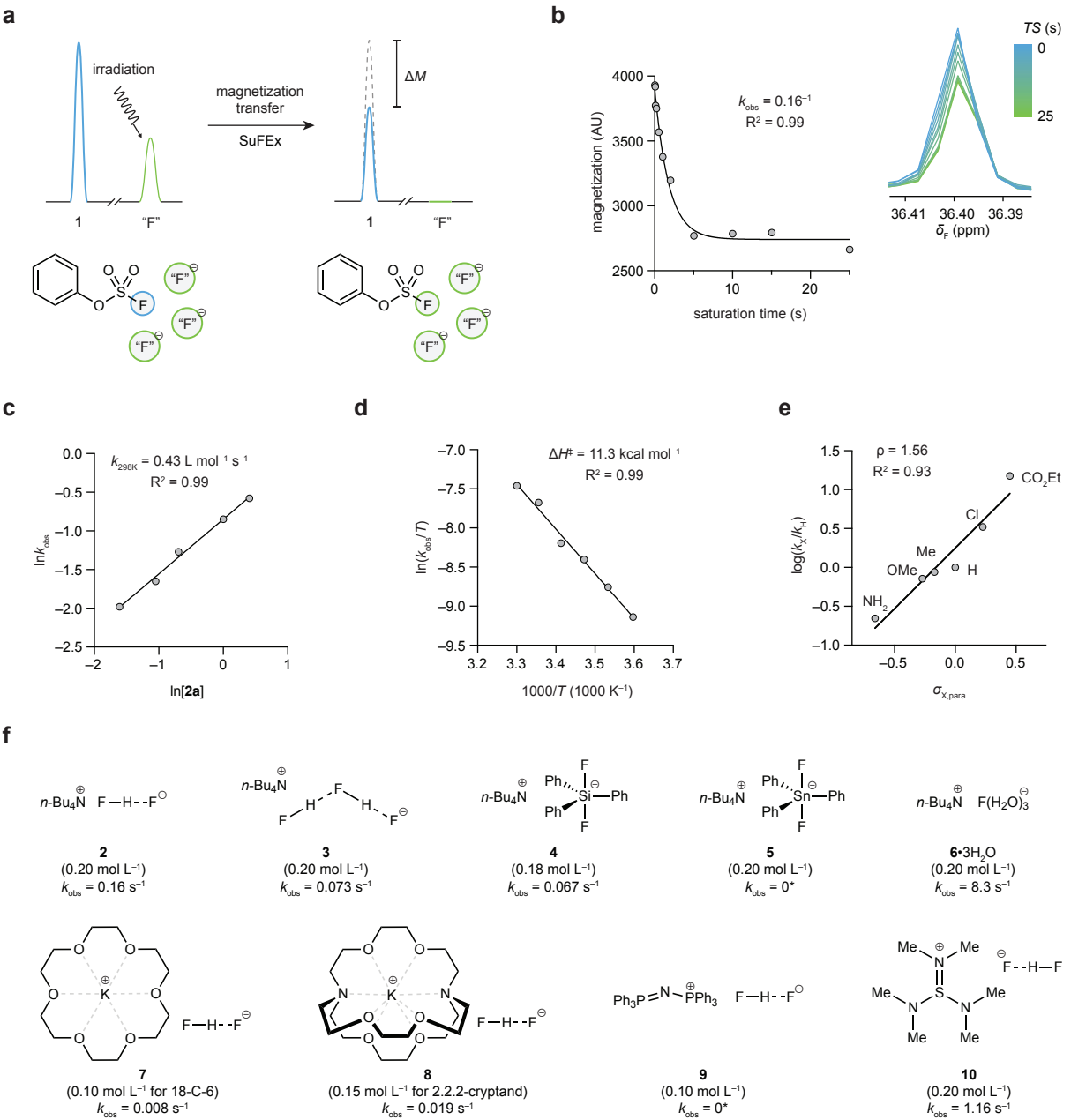
a
irradiation
magnetization transfer
SuFEx
ΔM
1
"F"
1
"F"
b
magnetization (AU)
4000
3500
3000
2500
0
10
20
saturation time (s)
k_{obs} = 0.16^{-1}
R^2 = 0.99
TS (s)
0
25
36.41
36.40
36.39
δ_F (ppm)
c
lnk_{obs}
k_{298K} = 0.43 L mol^{-1} s^{-1}
R^2 = 0.99
ln[2a]
d
ln(k_{obs}/T)
ΔH‡ = 11.3 kcal mol^{-1}
R^2 = 0.99
1000/T (1000 K^{-1})
e
log(k_X/k_H)
ρ = 1.56
R^2 = 0.93
CO$_2$Et
Cl
Me
OMe
H
NH$_2$
$\sigma_{X,para}$
f
n-Bu$_4$N F—H--F
2
(0.20 mol L^{-1})
k_{obs} = 0.16 s^{-1}
n-Bu$_4$N
3
(0.20 mol L^{-1})
k_{obs} = 0.073 s^{-1}
n-Bu$_4$N
4
(0.18 mol L^{-1})
k_{obs} = 0.067 s^{-1}
n-Bu$_4$N
5
(0.20 mol L^{-1})
k_{obs} = 0*
n-Bu$_4$N F(H$_2$O)$_3$
6•3H$_2$O
(0.20 mol L^{-1})
k_{obs} = 8.3 s^{-1}
F—H--F
7
(0.10 mol L^{-1} for 18-C-6)
k_{obs} = 0.008 s^{-1}
F—H--F
8
(0.15 mol L^{-1} for 2.2.2-cryptand)
k_{obs} = 0.019 s^{-1}
Ph$_3$P=N-PPh$_3$ F—H--F
9
(0.10 mol L^{-1})
k_{obs} = 0*
F--H—F
10
(0.20 mol L^{-1})
k_{obs} = 1.16 s^{-1}

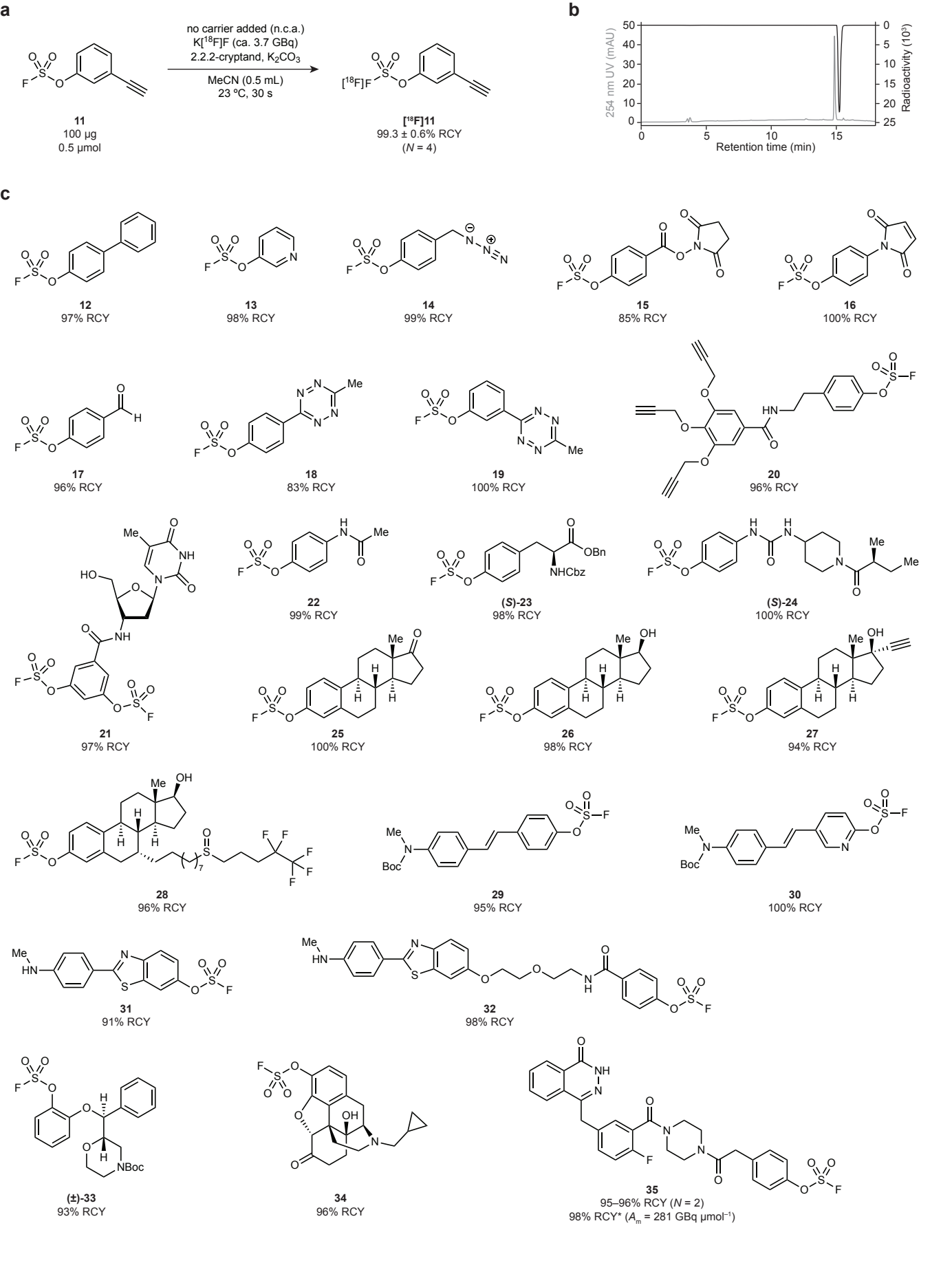
a
no carrier added (n.c.a.)
K[18F]F (ca. 3.7 GBq)
2.2.2-cryptand, K2CO3
MeCN (0.5 mL)
23 °C, 30 s
11
100 µg
0.5 µmol
[18F]11
99.3 ± 0.6% RCY
(N = 4)
b
254 nm UV (mAU)
Radioactivity (10³)
Retention time (min)
c
12
97% RCY
13
98% RCY
14
99% RCY
15
85% RCY
16
100% RCY
17
96% RCY
18
83% RCY
19
100% RCY
20
96% RCY
21
97% RCY
22
99% RCY
(S)-23
98% RCY
(S)-24
100% RCY
25
100% RCY
26
98% RCY
27
94% RCY
28
96% RCY
29
95% RCY
30
100% RCY
31
91% RCY
32
98% RCY
(±)-33
93% RCY
34
96% RCY
35
95–96% RCY (N = 2)
98% RCY* (Am = 281 GBq µmol−1)

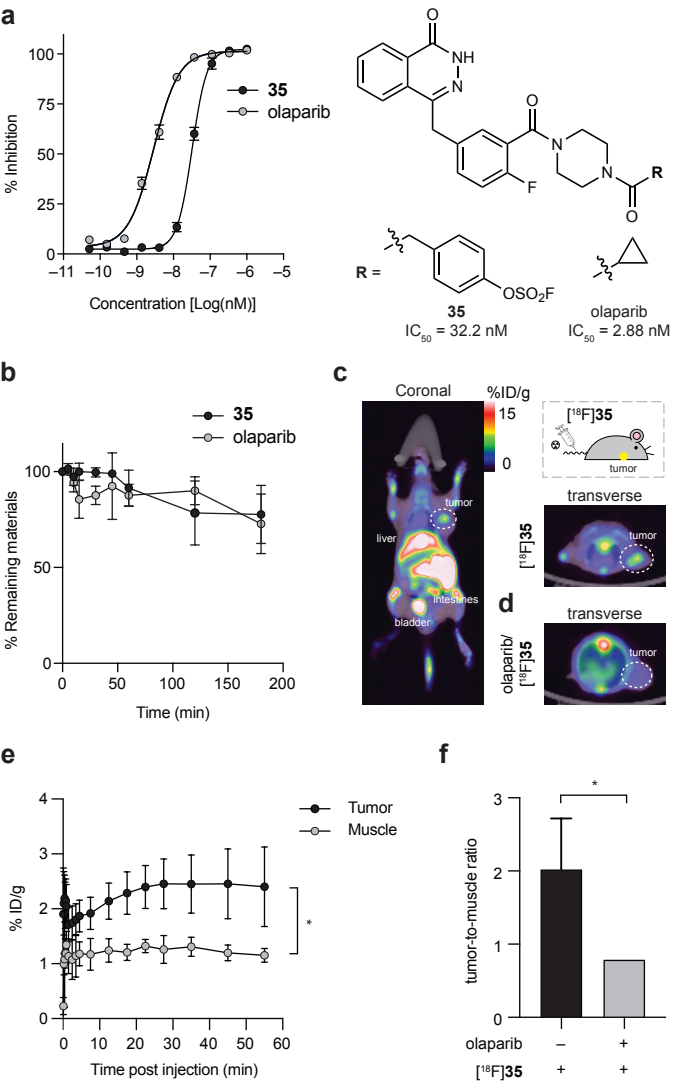
a
% Inhibition
100
75
50
25
0
−11 −10 −9 −8 −7 −6 −5
Concentration [Log(nM)]
35
olaparib
O
NH
N
O
N
N
R
F
O
R =
OSO2F
35
IC50 = 32.2 nM
olaparib
IC50 = 2.88 nM
b
35
olaparib
% Remaining materials
100
50
0
0 50 100 150 200
Time (min)
c
Coronal
%ID/g
15
0
tumor
liver
intestines
bladder
[18F]35
tumor
transverse
[18F]35
tumor
d
transverse
olaparib/
[18F]35
tumor
e
% ID/g
4
3
2
1
0
0 10 20 30 40 50 60
Time post injection (min)
Tumor
Muscle
*
f
tumor-to-muscle ratio
3
2
1
0
*
olaparib – +
[18F]35 + +